

Solving Inverse PDE Problems using Grid-Free Monte Carlo Estimators

EKREM FATIH YILMAZER, École Polytechnique Fédérale de Lausanne (EPFL), Switzerland

DELIO VICINI, École Polytechnique Fédérale de Lausanne (EPFL), Switzerland

WENZEL JAKOB, École Polytechnique Fédérale de Lausanne (EPFL), Switzerland

Modeling physical phenomena like heat transport and diffusion is crucially dependent on the numerical solution of partial differential equations (PDEs). A PDE solver finds the solution given coefficients and a boundary condition, whereas an *inverse PDE solver* goes the opposite way and reconstructs these inputs from an existing solution. In this article, we investigate techniques for solving inverse PDE problems using a gradient-based methodology.

Conventional PDE solvers based on the finite element method require a domain meshing step that can be fragile and costly. Grid-free Monte Carlo methods instead stochastically sample paths using variations of the *walk on spheres* algorithm to construct an unbiased estimator of the solution. The uncanny similarity of these methods to physically-based rendering algorithms has been observed by several recent works.

In the area of rendering, recent progress has led to the development of efficient unbiased derivative estimators. They solve an adjoint form of the problem and exploit arithmetic invertibility to compute gradients using a constant amount of memory and linear time complexity.

Could these two lines of work be combined to compute cheap parametric derivatives of a grid-free PDE solver? We investigate this question and present preliminary results.

CCS Concepts: • **Mathematics of computing** → **Partial differential equations**; • **Computing methodologies** → **Rendering**.

Additional Key Words and Phrases: walk on spheres, Monte Carlo, differentiable simulation, path replay backpropagation

1 INTRODUCTION

Many physical phenomena are naturally described using partial differential equations (PDEs). For example, the heat equation models the spread of thermal energy in a potentially heterogeneous material. Solvers that numerically approximate solutions of such PDEs are in widespread use. We pursue the opposite direction in this article, which is known as an *inverse PDE problem*: estimating unknown parameters from observations of the solution. This set of unknown parameters could include various PDE coefficients, boundary conditions, and even the shape of the domain.

Such problems arise in diverse scientific and engineering contexts, for example to determine the physical parameters of a thermal conductor from measurements [Cannon 1964]. Electrical impedance tomography [Cheney et al. 1999] seeks to reconstruct the interior of a living organism. Electrodes provide measurements of the electric field, which is influenced by the tissue’s conductivity, impedance, and dielectric permittivity.

Our approach entails differentiating the solver and recovering the unknown parameters using gradient descent. However, one issue with conventional PDE solvers based on the finite element method (FEM) is that they require a meshing step that can be fragile

and computationally costly. An alternative are Monte Carlo PDE solvers based on the *walk on spheres* (WoS) [Muller 1956]. These *grid-free* methods sample random paths in the domain to compute unbiased estimates of the solution. Grid-free solvers have recently attracted significant attention in the computer graphics community, partly owing to the remarkable similarities to Monte Carlo rendering methods [Sawhney and Crane 2020] and the algorithmic synergies that this creates [Sawhney et al. 2022; Qi et al. 2022].

A common issue with gradient-based optimization is that the standard approach for reverse-mode differentiation (known as *backpropagation*) reverses all data dependencies of an underlying computation. When applied to the WoS algorithm, this means that intermediate results of a large number of iterations would need to be stored to enable the subsequent differentiation.

In the field of rendering, recent progress has led to the development of *differentiable rendering* methods [Gkioulekas et al. 2013; Li et al. 2018; Nimier-David et al. 2019] that estimate parametric derivatives of complete light transport simulations. A similar issue arises here as well: light paths can potentially be very long, particularly in highly-scattering media, which makes naïve reverse-mode differentiation prohibitively memory-intensive. Methods like *radiative backpropagation* [Nimier-David et al. 2020] and *path replay backpropagation* [Vicini et al. 2021] cast the differentiation step into an independent simulation of “derivative light” to address this issue. The latter project solves an adjoint version of the underlying equation and furthermore exploits arithmetic invertibility in the computation to differentiate using a constant amount of memory and a runtime cost that is linear in the number of path vertices.

Given these striking similarities, could a similar approach be useful to compute reverse-mode derivatives of grid-free Monte Carlo solvers? We show that this is indeed the case and that this combination yields an unbiased derivative estimator in the same complexity class. The paper presents preliminary results on synthetic inverse problems. We make no claims about the utility of such an approach for solving concrete inverse-PDE problems but find it a promising direction for future work.

2 METHOD

2.1 Background

Inverse PDE problems. We seek to solve an inverse PDE problem of the form:

$$\hat{\pi} = \arg \min_{\pi} \ell(u(\pi)), \quad (1)$$

where $u(\pi)$ is the solution of a PDE parameterized by the vector π containing the boundary values, source terms, etc. The function ℓ is a differentiable objective function. In the simplest case, this could be the L_2 difference between the solution of the PDE and a reference solution evaluated at a set of locations spread throughout

Authors’ addresses: Ekrem Fatih Yilmazer, ekrem.yilmazer@epfl.ch, École Polytechnique Fédérale de Lausanne (EPFL), Lausanne, Switzerland; Delio Vicini, delio.vicini@epfl.ch, École Polytechnique Fédérale de Lausanne (EPFL), Lausanne, Switzerland; Wenzel Jakob, wenzel.jakob@epfl.ch, École Polytechnique Fédérale de Lausanne (EPFL), Lausanne, Switzerland.

the domain. We use a regular grid in experiments, though irregularly spaced evaluation points are also within the scope of this approach.

To attempt to solve this problem using gradient descent, we must differentiate the objective ℓ (and therefore, also the solver $u(\pi)$) with respect to π . For notational simplicity, we shall focus on a derivative $\partial_\pi := \partial/\partial\pi$ with respect to a single parameter π , though the resulting methods also generalize to arbitrary parameter counts.

Primal solver. The walk on spheres method [Muller 1956] expresses the solution $u(x, \pi)$ as a recursive integration problem. In this paper, we consider various PDEs which have a solution expressed as a *Fredholm integral equation of the second kind*:

$$u(x, \pi) = S(x, \pi) + \int_{\mathcal{Y}} K(x, x', \pi) u(x, \pi) dx'. \quad (2)$$

Here, \mathcal{Y} is typically a sphere around x and K attenuates the recursive contribution of u . The term S relates to the *source term* and is usually itself an integral that, however, does not reference the solution u . We assume both S and K to potentially depend on a differentiable parameter π . This formulation covers the range of PDEs described by recent works in computer graphics [Sawhney and Crane 2020; Sawhney et al. 2022]. The solution of the PDE can then efficiently be estimated using recursive Monte Carlo integration. We refer to Sawhney et al. [2020; 2022] for an in-depth introduction and discussion of walk on spheres.

This recursive formulation is reminiscent of the rendering equation [Kajiya 1986] solved by physically-based rendering algorithms:

$$L_o(x, \omega) = L_e(x, \omega) + \int_{S^2} f_s(x, \omega, \omega') L_i(x, \omega') d\omega'^\perp, \quad (3)$$

where L_o , L_i and L_e denote the outgoing, incident and emitted radiance and f is the *bidirectional scattering distribution function* (BSDF). In both equations, the solution appears recursively in the integral on the right. Both walk on spheres and rendering algorithms need to recursively sample the integrand on the right, potentially constructing long paths before terminating at a boundary or on a light source.

Derivative integrals. Instead of using a standard framework for automatic differentiation that would record the computational structure of the random walk at significant expense, recent differentiable rendering methods [Nimier-David et al. 2020; Vicini et al. 2021] cast the differentiation step into an independent random walk that propagates differential quantities (e.g., the derivative of radiance) through the domain.

These methods can be motivated by formulating the derivative of the solution by applying the derivative operator to Equation 2. Under the assumption that the parameter π does not affect the position of discontinuities in the integrand or the integration domain \mathcal{Y} itself, we then get:

$$\begin{aligned} \partial_\pi u(x, \pi) &= \partial_\pi S(x, \pi) + \partial_\pi \int_{\mathcal{Y}} K(x, x', \pi) u(x, \pi) dx' \\ &= \partial_\pi S(x, \pi) + \int_{\mathcal{Y}} \partial_\pi [K(x, x', \pi)] u(x, \pi) dx' \\ &\quad + \int_{\mathcal{Y}} K(x, x', \pi) \partial_\pi u(x, \pi) dx'. \end{aligned} \quad (4)$$

In contrast to the primal problem, we now have *two* recursive terms to estimate: both $\partial_\pi u$ and u require a separate random walk. In differentiable rendering, Nimier-David et al. [2020] suggested to recursively estimate both quantities, which results in quadratic complexity. We will instead use the path replay backpropagation algorithm [Vicini et al. 2021], which obtains the derivative in linear time.

In this paper, we will assume that the domain of the PDEs we solve is fixed. If that were not the case, \mathcal{Y} might be parameter dependent. In the simplest case, \mathcal{Y} is the largest sphere around x , which changes as the domain itself changes. We could then not simply move the derivative operator into the integral. We also assume that the functions S , K , as well as Dirichlet boundary values, are continuous. The discontinuous case has been studied in differentiable rendering and requires specialized techniques such as *edge sampling* [Li et al. 2018], *reparameterizations* [Loubet et al. 2019; Bangaru et al. 2020], or path-space edge sampling [Zhang et al. 2020]. We sidestep this point and focus on integrands that are continuous with respect to π . We leave the application of such techniques to PDEs with discontinuous parameters for future work.

2.2 Path replay backpropagation

In this paper, we adapt path replay backpropagation [Vicini et al. 2021] that applies to differential estimators of both Equations 2 and 3. The method is best explained using pseudocode. Algorithm 1 implements a simple primal solver for Equation 2:

```

1 def solve(x):
2   u = 0 # running solution estimate
3   beta = 1 # throughput
4   while not done:
5     u += beta * S(x, pi) # accumulate source term
6     x_new, pdf = sample_next_step(x)
7     beta *= K(x, x_new, pi) / pdf # update throughput
8     x = x_new
9   return u

```

Algorithm 1. Monte Carlo solver for a Fredholm equation of the second kind.

It computes a one-sample estimate of the solution at x . Initially, the running estimate u is set to 0 and the *throughput* β is set to 1. In each iteration, we accumulate the throughput-weighted source contribution (e.g., source term of the PDE or surface emission in rendering) and then sample the next position x , while updating the throughput using the ratio of K and the sampling PDF. In rendering, this would be the ratio of the BSDF and the solid angle density of the sampling strategy. The evaluation of S might also involve a Monte Carlo estimator, but this is usually simple as it does not recursively depend on u . If we were to use next event estimation, we would also consider it to be part of the evaluation of S in this context.

Path replay backpropagation can now be used to estimate derivatives in reverse mode. The central idea of this approach is to estimate the solution u and subsequently accumulate gradients by regenerating the *same path* a second time. In a concrete implementation, this would typically be accomplished by re-seeding the underlying source of pseudorandomness. When the path is reconstructed once more, the method can leverage the known final result to compute an unbiased gradient estimate. This involves no approximations and

removes the need to store large temporary buffers of intermediate random walk state.

The method evaluates a vector-Jacobian product $\delta_\pi = \delta_u^T J_s$, where J_s is the Jacobian of the solver in Algorithm 1. The vector δ_u contains the gradient of the objective function with respect to the value of u , and δ_π is the desired vector of parameter derivatives for gradient descent.

Algorithm 2 implements path replay backpropagation for the general solver in Algorithm 1:

```

1  def backward_solve(x, delta_u, u):
2      beta = 1
3      while not done:
4          with ad_enabled(): # Gradients of "S"
5              delta_pi += backward(beta * S(x, pi) * delta_u)
6
7          # no gradient is tracked outside of ad_enabled()
8          u -= beta * S(x, pi)
9          x_new, pdf = sample_next_step(x)
10         v = u / K(x, x_new, pi)
11         with ad_enabled(): # Gradients of "K"
12             delta_pi += backward(v * K(x, x_new, pi) * delta_u)
13         beta *= K(x, x_new, pi) / pdf
14         x = x_new

```

Algorithm 2. Path replay version of the Fredholm equation solver.

The function takes the query location x , the output of the first pass u and the objective function derivative δ_u as input. Here, we both evaluate the parameter-dependent functions S and K using automatic differentiation, and the function `backward` then backpropagates gradients into their parameters. By default, automatic differentiation eagerly propagates gradients through all involved quantities, but here we actually want to localize the usage of AD to consider only part of the loop body. Any computations outside the `ad_enabled()` blocks will not be differentiated by automatic differentiation. This also means that we never build an automatic differentiation graph across loop iterations, and hence do not need to allocate memory to store all the loop states. Note that the above pseudocode evaluates certain terms twice (e.g., $S(x, \pi)$). This is purely for notational clarity and in practice the same logic can be implemented using a single forward evaluation of these terms.

The above algorithm computes *detached* [Zeltner et al. 2021; Vicini et al. 2021] gradients, which means that we estimate the gradients of a parameter-dependent integral as:

$$\int_{\mathcal{X}} \partial_\pi f(x, \pi) dx \approx \frac{1}{N} \sum_{i=1}^N \frac{\partial_\pi f(x_i, \pi)}{p(x_i, \pi)}, \quad (5)$$

where N is a number of samples and x_i are i.i.d. samples with the probability density function $p(x_i)$. This estimator is detached in a sense that we do not differentiate the sampling strategy and PDF. We only differentiate the integrand f itself. On the other hand, *attached* estimators differentiate the sampling strategy, which is more expensive and requires additional precautions due to discontinuities [Zeltner et al. 2021]. In rendering, their use is limited to special cases such as perfectly specular surfaces. We use detached estimators throughout this paper, but attached estimators could potentially be useful to handle gradients with respect to the domain boundary.

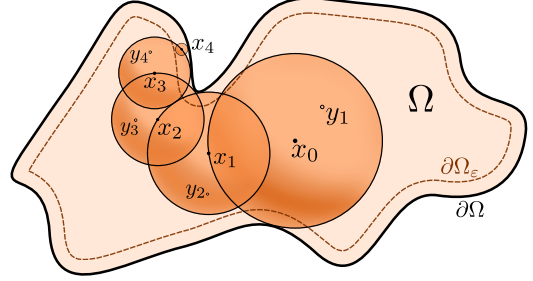


Fig. 1. Illustration of the steps taken by the walk on spheres estimator for the Poisson equation. Starting from a point x_0 , we repeatedly sample the next point x_i on the sphere around the current point until we sample a point inside Ω_ε . The set Ω_ε contains the points within ε -distance to the boundary $\partial\Omega$. Once we sample such a point, we evaluate the Dirichlet boundary values $g(x)$ and terminate the random walk. In each iteration, we further sample a point y_i to evaluate the source term f .

2.3 Poisson equation

The remainder of this article discusses different PDEs in turn: the Poisson equation (this section), its screened variant (Section 2.4), and the general case of a heterogeneous elliptic PDE (Section 2.5).

The Poisson equation is defined as

$$\begin{aligned} \Delta u(x) &= -f(x) & x \in \Omega, \\ u(x) &= g(x) & x \in \partial\Omega, \end{aligned} \quad (6)$$

where Ω is the domain, $\partial\Omega$ its boundary and u the solution function. The function $f(x)$ is a (spatially-varying) source term and $g(x)$ models the boundary values.

Primal estimator. The solution of the Poisson equation satisfies the following recursive equation [Sawhney and Crane 2020; DeLaurentis and Romero 1990]:

$$u(x) = \underbrace{\int_{B(x)} f(y)G(x, y) dy}_{=:S} + \underbrace{\frac{1}{|\partial B(x)|} \int_{\partial B(x)} u(z) dz}_{=:K}, \quad (7)$$

where $G(x, y)$ is the Green's function. Walk on spheres estimates $u(x)$ recursively by repeatedly sampling a point on a sphere $\partial B(x)$ around the current position until it reaches the boundary. For efficiency, we use the largest sphere that is still entirely contained inside the domain. Additionally, in each step we sample a position y inside the current sphere to evaluate the source term [Sawhney and Crane 2020]. This process is illustrated in Figure 1. A single sample of the walk on spheres estimator can be written as:

$$u(x) \approx \sum_{k=1}^N f(y_k)|G(x_k)| + g(x_N), \quad (8)$$

where $|G(x_k)| = \int_{B(x_k)} G(x_k, y) dy$ and $g(x_N)$ is the evaluation of the boundary condition at the point where we reach the domain boundary. We sample $y_k \in B(x_k)$ proportionally to the Green's function and $x_{k+1} \in \partial B(x_k)$ uniformly, which caused the terms $G(x_k, y_k)$ and $1/|\partial B(x_k)|$ to cancel in the above expression. Pseudocode for this estimator is shown in Algorithm 3. The function

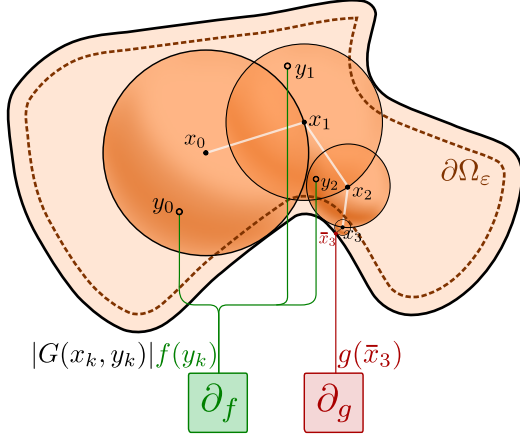


Fig. 2. Gradient computation for the Poisson equation. The colored (green, red) quantities are computed locally using automatic differentiation.

`poisson` estimates $u(x)$ for a given x , source term f and boundary values g . We compute the distance to the domain boundary inside `distance_to_boundary()`. The function `sample_green()` samples y proportionally to $G(x, y)$ and `sample_boundary()` uniformly samples the surface of the ball $B(x)$ of radius R .

```

1 def poisson(x, f, g):
2   u = 0
3   while True:
4     # Terminate walk once boundary is reached
5     R = distance_to_boundary(x)
6     if R < epsilon:
7       return u + g(x) # Evaluate boundary value and return
8
9     # Evaluate the source term
10    y = sample_green(x, R)
11    u += f(y) * |G(x)|
12
13    # Sample next point on partial B(x)
14    x = sample_boundary(x, R)

```

Algorithm 3. Walk on spheres for the Poisson equation.

Differential WoS. The Poisson equation solver is the easiest to differentiate. Later sections will require the use of *path replay* to regenerate a random walk twice, but it is not needed here. This is because the throughput of the sampled path is not parameter dependent.

The estimator in Equation 8 computes a weighted sum of f and g -evaluations. To differentiate it, we must evaluate the reverse-mode derivative of all terms in this sum. Algorithm 4 implements this computation using a *differential walk on spheres* (dWoS), which is illustrated in Figure 2.

2.4 Screened Poisson equation

The *screened* Poisson problem presents a slightly more complex case. This PDE includes an extra scalar screening coefficient σ :

$$\begin{aligned} \Delta u(x) - \sigma u(x) &= -f(x) & x \in \Omega, \\ u(x) &= g(x) & x \in \partial\Omega. \end{aligned} \quad (9)$$

```

1 def backward_poisson(x, delta_u, f, g):
2   while True:
3     R = distance_to_boundary(x)
4     if R < epsilon:
5       with ad_enabled():
6         delta_pi += backward(delta_u * g(x))
7       return delta_pi
8
9     y = sample_green(x, R)
10    with ad_enabled():
11      delta_pi += backward(delta_u * f(y) * |G(x)|)
12
13    x = sample_boundary(x, R)

```

Algorithm 4. Differential walk on spheres for the Poisson equation.

Its solution satisfies the following Fredholm integral equation [Sawhney and Crane 2020; Elepov and Mikhailov 1969]:

$$u(x) = \underbrace{\int_{B(x)} f(y) G^\sigma(x, y) dy}_{=:S} + \underbrace{\int_{\partial B(x)} P^\sigma(x, z) u(z) dz}_{=:K}, \quad (10)$$

where $P^\sigma(x, z)$ is the Poisson kernel and $G^\sigma(x, y)$ is the harmonic Green's function of $B(x)$ (see Appendix A for the definition of these functions). Both the Green's function and the Poisson kernel depend on the screening coefficient σ . The sampling strategy remains unchanged: we sample the Green's function to estimate the source term and draw uniform locations on the sphere boundary to obtain the next path vertex. However, the value of the Poisson kernel does not cancel with the sampling PDF and we thus end up with a parameter-dependent throughput term.

Path replay is now necessary to efficiently differentiate this estimator in reverse mode. Matching pseudocode is shown in Algorithm 5. The structure largely resembles Algorithm 5, but the function now takes the result of a previous primal solution estimate as input (variable u). In each step, the current source term evaluation is subtracted from u (Line 15), which is then used to compute the gradient of the throughput update (Line 20). The quantities used during the reverse-mode gradient computation are illustrated in Figure 3.

2.5 General heterogeneous elliptic problems

The screened Poisson problem required the use of path replay to estimate gradients of the screening coefficient. However, the use of path replay for this problem was mainly pedagogical: since the screening coefficient is just a scalar, one could easily estimate its derivative using forward-mode AD or even finite differences.

Sawhney et al. [2022] propose WoS-based solvers supporting spatially varying PDE coefficients building on methods from volumetric transport. We analyze their delta tracking-based approach and derive the corresponding differential estimator. The algorithms target elliptic PDEs of the form

$$\begin{aligned} \nabla(\alpha(x)\nabla u(x)) + \vec{\omega}(x)\nabla u(x) - \sigma(x)u(x) &= -f(x) & x \in \Omega \\ u(x) &= g(x) & x \in \partial\Omega. \end{aligned} \quad (11)$$

```

1 def backward_screened_poisson(x, delta_u, u, f, g, sigma):
2     beta = 1
3     while True:
4         R = distance_to_boundary(x)
5         if R < epsilon:
6             with ad_enabled():
7                 delta_pi += backward(delta_u * beta * g(x))
8                 return delta_pi
9
10        # Source term gradient
11        y, pdf_green = sample_green(x, R, sigma)
12        with ad_enabled():
13            S = beta * f(y) * G(x, y, sigma) / pdf_green
14            delta_pi += backward(S * delta_u)
15        u -= S # no gradient is tracked outside of ad_enabled()
16
17        # Throughput gradient due to |sigma|
18        u_in = u / P(x, R, sigma)
19        with ad_enabled():
20            delta_pi += backward(u_in * P(x, R, sigma) * delta_u)
21
22        x, pdf_boundary = sample_boundary(x, R)
23        beta *= P(x, R, sigma) / pdf_boundary

```

Algorithm 5. Differential walk on spheres with path replay for the screened Poisson equation.

Here, $\alpha(x)$, $\omega(x)$ and $\sigma(x)$ are spatially variable diffusion, transport and screening coefficients. Similar to Sawhney et al. [2022], we also assume $\vec{\omega}(x) = 0$ for simplicity. That said, the general principles shown here could be used to develop primal and differential estimators that furthermore account for this term.

The integral formulation for this general elliptic PDE is:

$$u(x) = \int_{B(x)} f(y) \sqrt{\frac{1}{\alpha(x)\alpha(y)}} G^{\bar{\sigma}}(x, y) dy \quad (\text{T1})$$

$$+ \int_{B(x)} (\bar{\sigma} - \sigma'(z)) \sqrt{\frac{\alpha(z)}{\alpha(x)}} u(y) G^{\bar{\sigma}}(x, z) dz \quad (\text{T2})$$

$$+ \int_{\partial B(x)} \sqrt{\frac{\alpha(z)}{\alpha(x)}} u(z) P(x, z) dy \quad (\text{T3}) \quad (12)$$

where $\bar{\sigma}$ is a non-zero fictitious screening coefficient and σ' is defined as:

$$\sigma'(x) := \frac{\sigma(x)}{\alpha(x)} + \frac{1}{2} \left[\frac{\Delta \alpha(x)}{\alpha(x)} - \frac{1}{2} |\nabla \log(\alpha(x))|^2 \right] \quad (13)$$

This integral form is similar to the integral formulation of delta tracking [Woodcock et al. 1965; Galtier et al. 2013]. When estimating $u(x)$ using walk on spheres, the source term (T1) is evaluated as before. However, similar to delta tracking, only one of the terms T2 and T3 is sampled in each step. This is crucial to avoid quadratic complexity in the number of interactions. Sawhney et al. [2022] derived suitable sampling probabilities for each term.

Differential WoS. Since in each step we only sample one of the recursive terms in Equation 12, we can apply path replay just like before. During the gradient computation phase, we will sample both terms in the exact same sequence as during the primal phase.

Intuitively, the discrete sampling decision to either sample T2 or T3 might appear problematic, as it is non-differentiable. However,

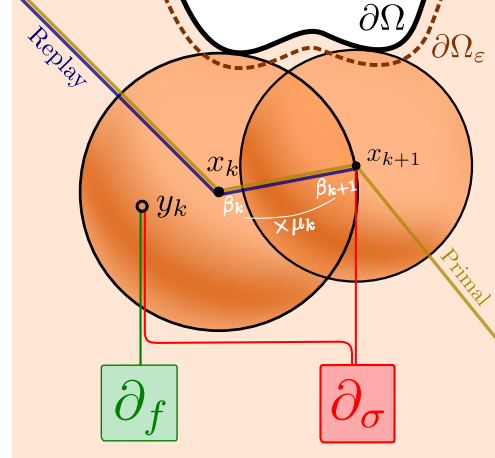


Fig. 3. Path replay WoS algorithm of the screened Poisson equation (k 'th iteration). The colored (green, red) lines indicate the positions where the gradients are accumulated.

our *detached* estimator does not need to differentiate the sampling process itself. As the integrand remains continuous, there is no issue differentiating the general elliptic WoS estimator. In rendering, the same reasoning was used to differentiate delta tracking using path replay [Vicini et al. 2021].

The pseudocode of the algorithm is given in Algorithm 6. Analogous to the differential WoS for the screened Poisson equation, the function uses the previous solution estimate u . As before, we subtract the source term contribution from it in each iteration (Line 15). In Line 18 we decide whether to sample the volume term T2 or the area term T3. The function sampler `.rand()` returns a random number that is uniformly distributed in $[0, 1)$. As suggested by Sawhney et al. [2022], we sample the volume term with a probability $|G(x)|\bar{\sigma}$. The new position x_{new} is then sampled by either sampling the Green's function or uniformly sampling of the sphere surface. In the following lines 26-30, we compute the multiplicative throughput change μ with AD enabled. In the notation of the original Fredholm equation solver, μ corresponds to the ratio of the evaluation of K and the sampling PDF. We then backpropagate gradients through μ , weighted by the loss gradient and u divided by the *detached* μ . Here, the function `detach(x)` disconnects its argument from the automatic differentiation graph. This allows writing Algorithm 2 without duplicating the computation of μ once inside and once outside the `ad_enabled()` block.

3 RESULTS

Gradient validation. We first validate the correctness of our gradient computations against finite differences. In Figure 4, we validate the source term gradient for the screened Poisson solution. The objective function is simply the L_2 norm of the solution image and the source function f is a cubically-interpolated 16×16 texture.

In Figure 5, we show a similar comparison for the general elliptic PDE. The objective function is again the L_2 norm of the solution image and we differentiate with respect to the source term f , screening coefficient σ and diffusion coefficient α . The gradients constructed

```

1 def path_replay_delta(x, u,  $\delta_u$ , f, g,  $\sigma$ ,  $\bar{\sigma}$ ,  $\alpha$ ):
2      $\beta = 1$ 
3     while True:
4         R = distance_to_boundary(x)
5         if R <  $\epsilon$ :
6             with ad_enabled():
7                  $\delta_\pi +=$  backward( $\delta_u * \beta * g(x)$ )
8             return  $\delta_\pi$ 
9
10        # Evaluate source contribution gradient
11        y, pdf_green = sample_green(x, R,  $\bar{\sigma}$ )
12        with ad_enabled():
13            S =  $\beta * f(y) * |G(x)| / \text{sqrt}(\alpha(x) * \alpha(y))$ 
14             $\delta_\pi +=$  backward( $\delta_u * S$ )
15        u -= S
16
17        # Decide sampling between boundary and volume.
18        sample_volume = sampler.rand() <  $|G(x)| * \bar{\sigma}$ 
19        if sample_volume:
20            x_new = sample_green(x, R,  $\bar{\sigma}$ )
21        else:
22            x_new = sample_boundary(x, R)
23
24        # Evaluate throughput and its gradient
25        with ad_enabled():
26             $\mu = \text{sqrt}(\alpha(x_{\text{new}}) / \alpha(x))$ 
27            if sample_volume:
28                 $\sigma' = \text{eval\_}\sigma'(\sigma(x_{\text{new}}), \alpha(x_{\text{new}}),$ 
29                     $\nabla\alpha(x_{\text{new}}), \Delta\alpha(x_{\text{new}}))$ 
30                 $\mu *= 1.0 - \sigma' / \bar{\sigma}$ 
31            v = u / detach( $\mu$ )
32             $\delta_\pi +=$  backward( $\delta_u * \mu * v$ )
33
34         $\beta *= \mu$ 
35        x = x_new

```

Algorithm 6. Differential walk on spheres using delta tracking for the general elliptic PDE.

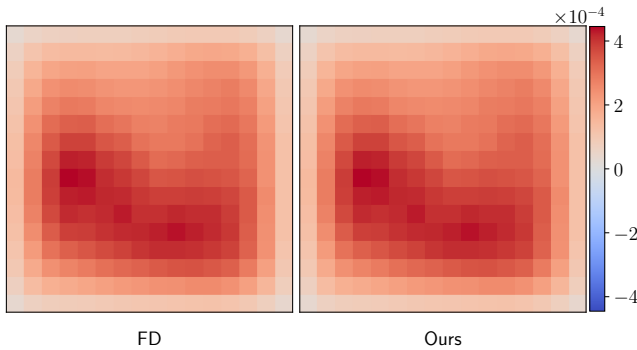


Fig. 4. Validation of the source term gradient of the screened Poisson equation against finite differences (FD). The screening coefficient is set to 10. See Figure 7 for a visualization of the used source term and PDE solution.

using path replay perfectly match the finite difference reference, which confirms that our estimator is indeed correct. The parameters for this experiment are visualized in Figure 8.

Optimizations. We demonstrate the use of our gradient estimators on a few example problems in 2D. We optimize various coefficients to minimize the L_2 error compared to the reference. In each experiment we optimize one parameter represented by a regular 2D texture.

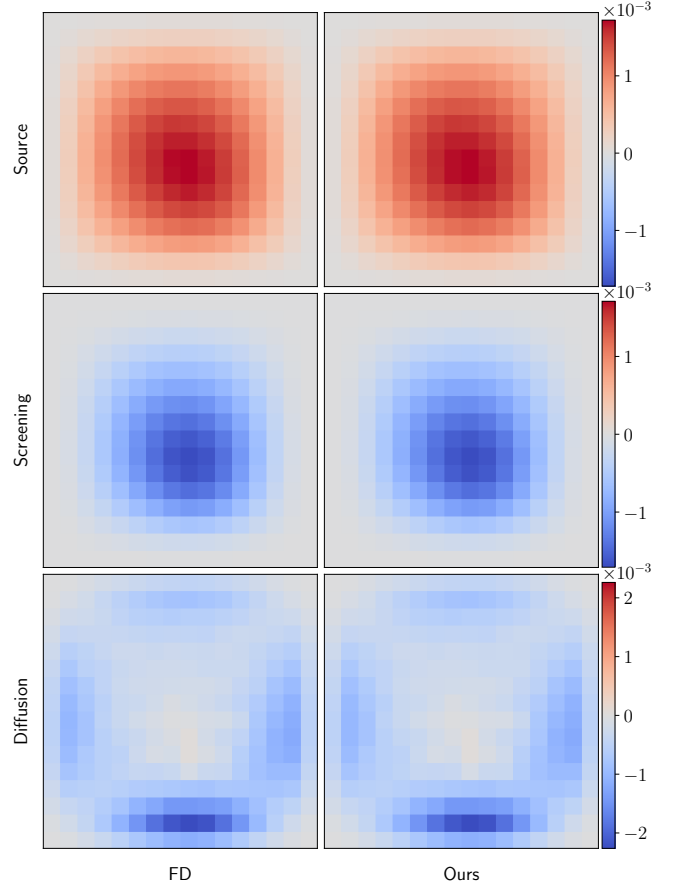


Fig. 5. Comparison between our delta tracking gradient estimate and the finite differences reference for the various parameters of the general elliptic PDE.

Figure 6 shows the optimization results and plots of the objective function values for three example problems. For all three problems, the error decreases as the optimization progresses. However, this does not necessarily guarantee that the recovered parameters match the reference parameters. Although some inverse PDE problems admit unique solutions [Isakov 2006], the elliptic problems discussed here are inherently ambiguous, so any practical application most likely will require using a prior or regularization.

The reconstruction of the source coefficient is the least vulnerable to these ambiguities. As seen from the result in Figure 6, the optimized source coefficient is almost identical to the reference source image in the region of interest. This is consistent with observations made in differentiable rendering, where emissive representations (e.g., neural radiance fields [Mildenhall et al. 2020]) are easier to optimize than general physically-based scene representations.

The optimization of the screening coefficient is partially successful in the sense that the general shape of the reference screening σ texture is recovered. The reconstruction of the diffusion coefficient α appears to be the least convex of our examples. In our experiments with different setups, we observed that the diffusion coefficients can

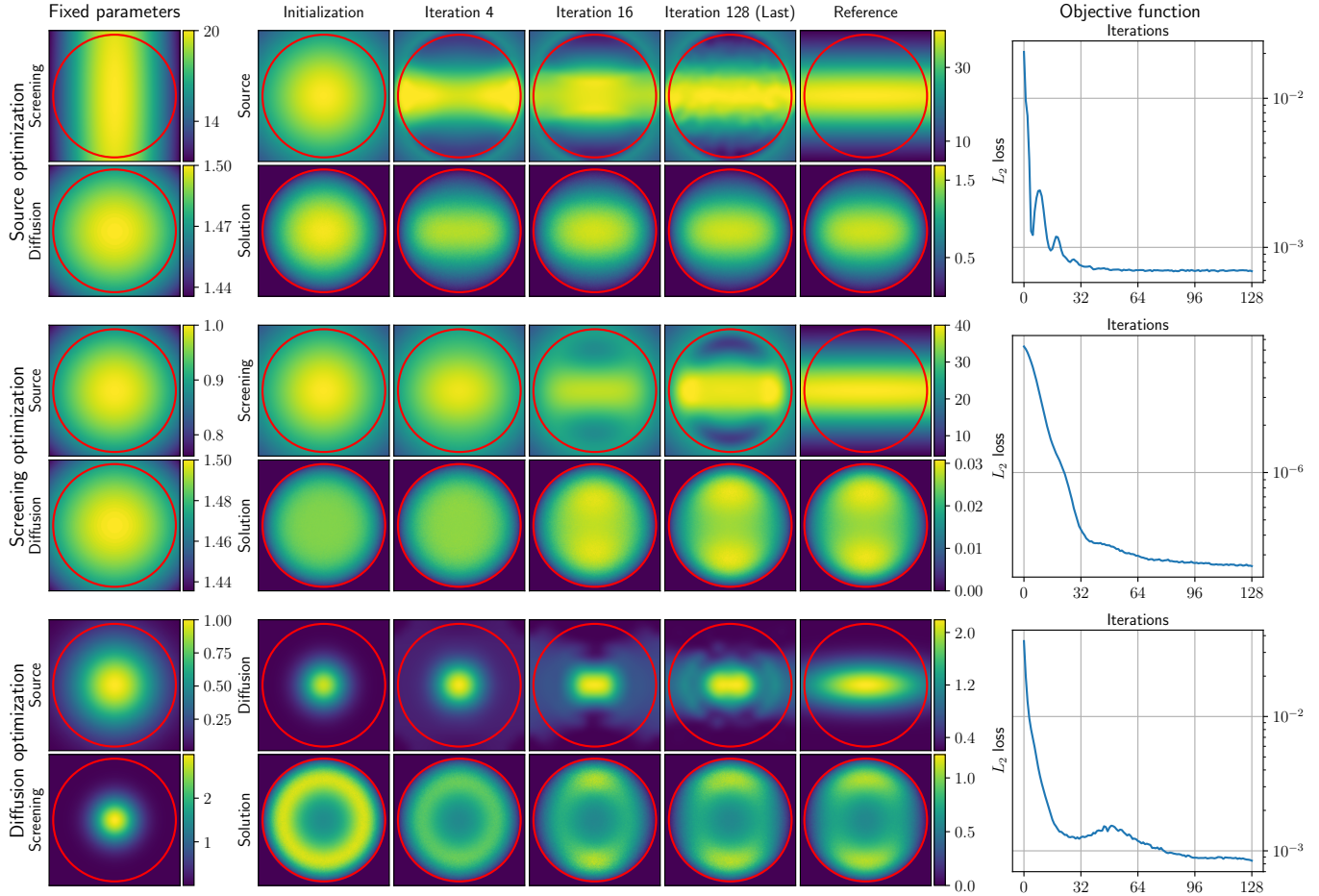


Fig. 6. Optimization results for optimizing source term, screening coefficient and diffusion coefficient using the differential delta tracking WoS.

evolve in a way that the overall shape of the texture is quite different from the reference coefficient, although the optimized and the reference solutions are comparable. In all optimizations, the solution of the PDE after optimization closely matches the reference.

4 CONCLUSION AND FUTURE WORK

The main objective of this paper was to build differentiable Monte Carlo estimators for solving inverse problems of PDEs. We proposed differential walk on spheres algorithms for the types of PDEs discussed by Sawhney et al. [2020; 2022]. Our methods are unbiased and require a constant amount of memory. Their complexity is linear in the number of sphere steps. We also provided some preliminary optimization results which indicate that the differentiable Monte Carlo PDE solvers have the potential to solve a range of inverse PDE problems.

As solving inverse problems of PDEs using differentiable Monte Carlo is a new approach, there are many future directions to explore. It would be interesting to also compute gradients with respect to the domain boundary. This could be done using an attached version of PRB, as previously demonstrated for specular surfaces [Vicini et al. 2021]. Further development of inverse Monte Carlo PDE methods

would benefit from experiments on real-world problems, which could highlight where our methods still lack. In particular, it would be interesting to combine our approach with application-specific priors and regularization to overcome local minima and ambiguities.

ACKNOWLEDGMENTS

We thank Rohan Sawhney and Dario Seyb for sharing the implementation of their primal solvers with us. We further thank Ziyi Zhang for proofreading. This research was supported by the Swiss National Science Foundation (SNSF) as part of grant 200021_184629.

REFERENCES

- Sai Bangaru, Tzu-Mao Li, and Frédo Durand. 2020. Unbiased Warped-Area Sampling for Differentiable Rendering. *ACM Trans. Graph. (Proc. SIGGRAPH Asia)* 39, 6 (2020), 245:1–245:18.
- J.R Cannon. 1964. Determination of certain parameters in heat conduction problems. *J. Math. Anal. Appl.* 8, 2 (1964), 188–201.
- Margaret Cheney, David Isaacson, and Jonathan C. Newell. 1999. Electrical Impedance Tomography. *SIAM Rev.* 41, 1 (1999), 85–101.
- John M DeLaurentis and Louis A Romero. 1990. A Monte Carlo method for Poisson's equation. *J. Comput. Phys.* 90, 1 (1990), 123–140.
- B.S. Elepov and G.A. Mikhailov. 1969. Solution of the dirichlet problem for the equation $\Delta u - cu = -q$ by a model of "walks on spheres". *U. S. S. R. Comput. Math. and Math. Phys.* 9, 3 (1969), 194–204. [https://doi.org/10.1016/0041-5553\(69\)90070-6](https://doi.org/10.1016/0041-5553(69)90070-6)

- Mathieu Galtier, Stéphane Blanco, Cyril Caliot, Christophe Coustet, Jérémie Dauchet, Mouna El Hafi, Vincent Eymet, Richard Fournier, Jacques Gautrais, Anaïs Khuong, et al. 2013. Integral formulation of null-collision Monte Carlo algorithms. *Journal of Quantitative Spectroscopy and Radiative Transfer* 125 (2013).
- Ioannis Gkioulekas, Shuang Zhao, Kavita Bala, Todd Zickler, and Anat Levin. 2013. Inverse Volume Rendering with Material Dictionaries. *ACM Trans. Graph. (Proc. SIGGRAPH Asia)* 32, 6, Article 162 (Nov. 2013).
- Victor Isakov. 2006. *Inverse problems for partial differential equations*. Springer.
- James T Kajiya. 1986. The rendering equation. In *Proceedings of the 13th annual conference on Computer graphics and interactive techniques*. 143–150.
- Tzu-Mao Li, Miika Aittala, Frédo Durand, and Jaakko Lehtinen. 2018. Differentiable Monte Carlo Ray Tracing through Edge Sampling. *ACM Trans. Graph. (Proc. SIGGRAPH Asia)* 37, 6 (2018), 222:1–222:11.
- Guillaume Loubet, Nicolas Holzschuch, and Wenzel Jakob. 2019. Reparameterizing discontinuous integrands for differentiable rendering. *Transactions on Graphics (Proceedings of SIGGRAPH Asia)* 38, 6 (Dec. 2019).
- Ben Mildenhall, Pratul P. Srinivasan, Matthew Tancik, Jonathan T. Barron, Ravi Ramamoorthi, and Ren Ng. 2020. NeRF: Representing Scenes as Neural Radiance Fields for View Synthesis. In *ECCV*. 25 pages.
- Mervin E. Muller. 1956. Some Continuous Monte Carlo Methods for the Dirichlet Problem. *The Annals of Mathematical Statistics* 27, 3 (1956), 569 – 589. <https://doi.org/10.1214/aoms/1177728169>
- Merlin Nimier-David, Sébastien Speierer, Benoît Ruiz, and Wenzel Jakob. 2020. Radiative Backpropagation: An Adjoint Method for Lightning-Fast Differentiable Rendering. *ACM Trans. Graph. (Proc. SIGGRAPH)* 39, 4 (July 2020). <https://doi.org/10.1145/3386569.3392406>
- Merlin Nimier-David, Delio Vicini, Tizian Zeltner, and Wenzel Jakob. 2019. Mitsuba 2: A Retargetable Forward and Inverse Renderer. *ACM Trans. Graph. (Proc. SIGGRAPH Asia)* 38, 6 (Nov. 2019), 17 pages.
- Yang Qi, Dario Seyb, Benedikt Bitterli, and Wojciech Jarosz. 2022. A bidirectional formulation for Walk on Spheres. *Computer Graphics Forum (Proceedings of EGSR)* 41, 4 (July 2022). <https://doi.org/10.1111/cgf.14586>
- Rohan Sawhney and Keenan Crane. 2020. Monte Carlo geometry processing: A grid-free approach to PDE-based methods on volumetric domains. *ACM Transactions on Graphics* 39, 4 (2020).
- Rohan Sawhney, Dario Seyb, Wojciech Jarosz, and Keenan Crane. 2022. Grid-free Monte Carlo for PDEs with spatially varying coefficients. *ACM transactions on graphics* 41, 4 (2022).
- Delio Vicini, Sébastien Speierer, and Wenzel Jakob. 2021. Path Replay Backpropagation: Differentiating Light Paths using Constant Memory and Linear Time. *ACM Trans. Graph. (Proc. SIGGRAPH)* 40, 4 (Aug. 2021), 108:1–108:14. <https://doi.org/10.1145/3450626.3459804>
- E Woodcock, T Murphy, P Hemmings, and S Longworth. 1965. Techniques used in the GEM code for Monte Carlo neutronics calculations in reactors and other systems of complex geometry. In *Proc. Conf. Applications of Computing Methods to Reactor Problems*, Vol. 557.
- Tizian Zeltner, Sébastien Speierer, Iliyan Georgiev, and Wenzel Jakob. 2021. Monte Carlo Estimators for Differential Light Transport. *ACM Trans. Graph. (Proc. SIGGRAPH)* 40, 4 (Aug. 2021). <https://doi.org/10.1145/3450626.3459807>
- Cheng Zhang, Bailey Miller, Kai Yan, Ioannis Gkioulekas, and Shuang Zhao. 2020. Path-Space Differentiable Rendering. *ACM Trans. Graph.* 39, 4 (2020), 143:1–143:19.

A GREEN’S FUNCTIONS AND POISSON KERNELS

For completeness, we recapitulate the formulats for for the Green’s functions and the Poisson kernels in 2D and 3D. The Green’s functions on the ball $B(x)$ are:

$$G_{2D}^{\sigma}(x, y) = \frac{1}{2\pi} \left[K_0(r\sqrt{\sigma}) - \frac{K_0(R\sqrt{\sigma})}{I_0(R\sqrt{\sigma})} I_0(r\sqrt{\sigma}) \right]$$

$$G_{3D}^{\sigma}(x, y) = \frac{1}{4\pi} \left[\frac{e^{-r\sqrt{\sigma}}}{r} - \frac{e^{-R\sqrt{\sigma}}}{R} \left(\frac{\sinh(r\sqrt{\sigma})}{r\sqrt{\sigma}} - \frac{R\sqrt{\sigma}}{\sinh(R\sqrt{\sigma})} \right) \right]$$

where r is the Euclidian distance between x and y , R is the radius of the ball $B(x)$, I_0 and K_0 are the zeroth order modified Bessel functions of the first and the second kind. The integral of the Green’s function over the ball $B(x)$ is used to compute the PDF of sampling

proportional to it:

$$|G_{2D}^{\sigma}(x)| = \int_{B(x)} G_{2D}^{\sigma}(x, y) dy = \frac{1}{\sigma} \left[1 - \frac{1}{I_0(R\sqrt{\sigma})} \right]$$

$$|G_{3D}^{\sigma}(x)| = \int_{B(x)} G_{3D}^{\sigma}(x, y) dy = \frac{1}{\sigma} \left[1 - \frac{R\sqrt{\sigma}}{\sinh(R\sqrt{\sigma})} \right]$$

The Poisson kernel is the derivative of the Green’s function along the normal of the boundary:

$$P_{2D}^{\sigma}(x, z) = \frac{1}{2\pi R} \left[\frac{1}{I_0(R\sqrt{\sigma})} \right]$$

$$P_{3D}^{\sigma}(x, z) = \frac{1}{4\pi R^2} \left[\frac{R\sqrt{\sigma}}{\sinh(R\sqrt{\sigma})} \right]$$

The Poisson kernel is equal to $\frac{1-\sigma|G^{\sigma}(x)|}{|\partial B(x)|}$, which is a key property used in the derivation of the delta tracking WoS.

B INPUT CONFIGURATIONS OF THE GRADIENT VALIDATION

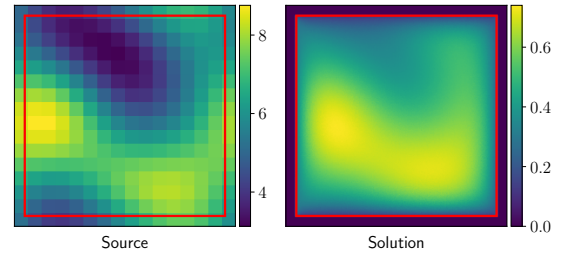


Fig. 7. Input configuration of the finite difference test for the screened Poisson equation. Boundaries are indicated with red lines and all boundary values are set to zero. The screening coefficient σ is set to 10.

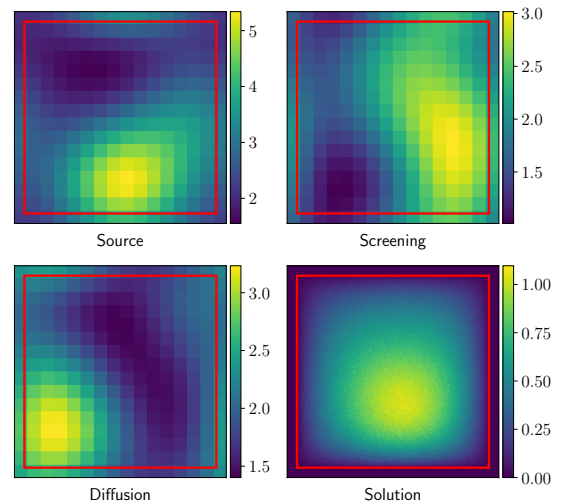


Fig. 8. Input configuration of the finite difference test of the delta tracking WoS. Boundaries are indicated with red lines and all boundary values are set to zero.

C PARAMETER GRADIENTS

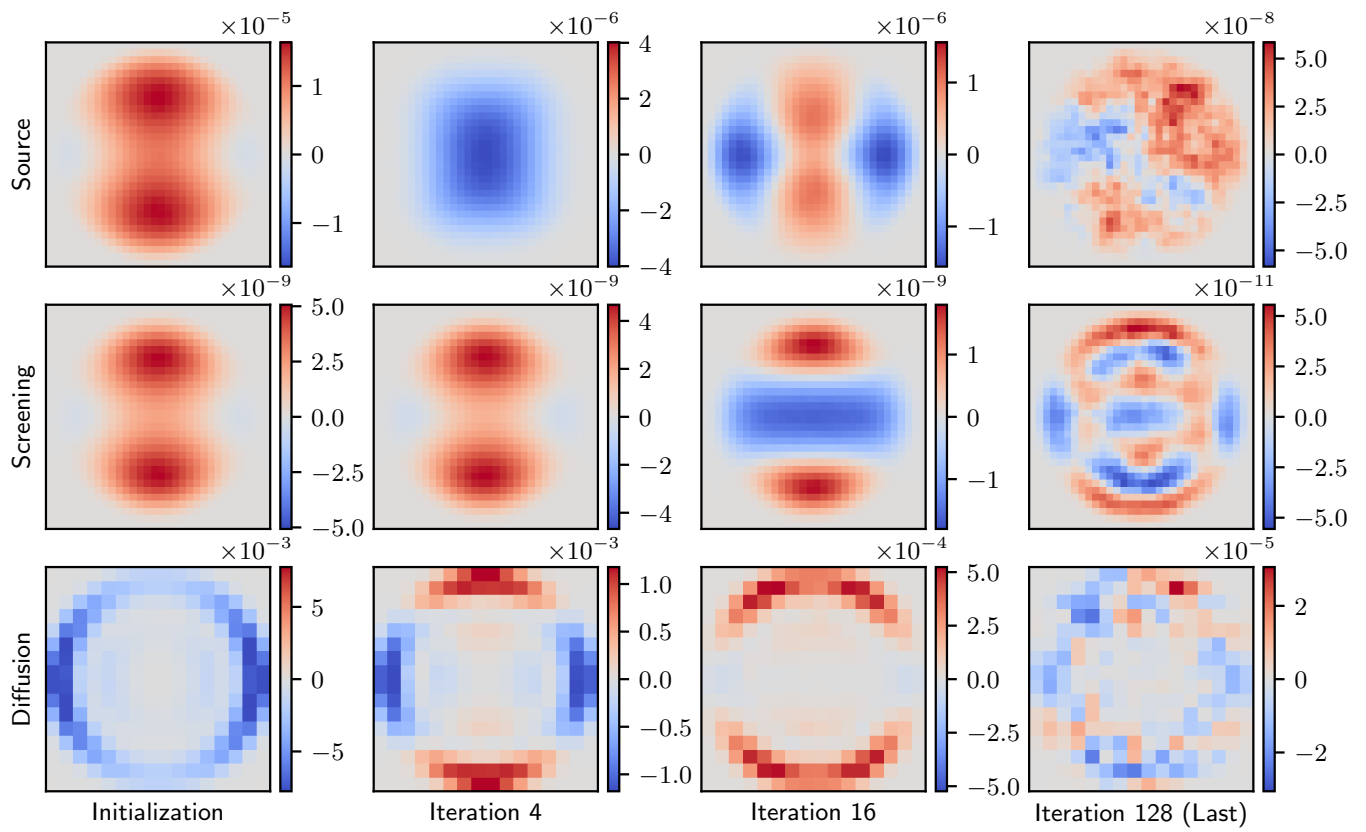


Fig. 9. Visualization of the parameter gradients for different optimization iterations. As the optimizations progress, the objective function value and hence the magnitude of the parameter gradients decreases.